EARTHQUAKE ENGINEERING AND STRUCTURAL DYNAMICS
Earthquake Engng Struct. Dyn. 2000; **29**:745–768

Time-domain viscoelastic analysis of earth structures

Nicos Makris*,† and Jian Zhang‡

Department of Civil and Environmental Engineering, University of California, Berkeley, CA 94720-1710, U.S.A.

SUMMARY

In this paper two causal models that approximate the nearly frequency-independent cyclic behaviour of soils are analysed in detail. The study was motivated by the need to conduct time-domain viscoelastic analysis on soil structures without adopting the ad hoc assumption of Rayleigh damping. First, the *causal hysteretic model* is introduced in which its imaginary part is frequency independent the same way that is the imaginary part of the popular non-causal *constant hysteretic model*. The adoption of an imaginary part that is frequency independent even at the zero-frequency limit, in conjunction with the condition that the proposed model should be causal, yields a real part that is frequency dependent and singular at zero frequency. The paper shows that the causal hysteretic model, although pathological at the static limit, is the mathematical connection between the non-causal constant hysteretic model and the physically realizable *Biot model*. The mathematical structure of the two causal models is examined and it is shown that the causal hysteretic model is precisely the high-frequency limit of the Biot model. Although both models have a closed-form time-domain representation, only the Biot model is suitable for a time-domain viscoelastic analysis with commercially available computer software. The paper demonstrates that the simplest, causal and physically realizable linear hysteretic model that can approximate the cyclic behaviour of soil is the Biot model.

The proposed study elucidates how the dynamic analysis of soil structures can be conducted rigorously in terms of the viscoelastic properties of the soil material and not with the ad hoc Rayleigh damping approach which occasionally has been criticized that tends to overdamp the higher vibration modes. The study concludes that under pulse-type motions the Rayleigh damping approximation tends to overestimate displacements because of the inappropriate viscous type of dissipation that is imposed. Under longer motions that induce several cycles, the concept of equivalent viscous damping is more appropriate and the Rayleigh damping approximation results to a response that is comparable to the response computed with a rigorous time-domain viscoelastic finite element analysis. Copyright © 2000 John Wiley & Sons, Ltd.

KEY WORDS: time-domain viscoelastic analysis; hysteretic behaviour; causality; soil structures

INTRODUCTION

Early experimental studies in soil dynamics indicated that the dissipative stresses that develop in sands when subjected to small-amplitude vibrations are nearly frequency independent. This

* Correspondence to: Nicos Makris, Department of Civil Engineering, University of California, Berkeley, CA 94720-1710, U.S.A.
† Associate Professor
‡ Graduate Research Assistant

Received 29 April 1999
Revised 12 November 1999
Accepted 16 November 1999

frequency independence suggests that energy loss in sands, and generally in soils, is not of viscous type; and Hardin [1] proposed a modification of the standard Kelvin–Voight model in which the viscosity is assumed to decrease with frequency such that the ratio viscosity times frequency divided by shear modulus is constant with frequency. The simple model proposed by Hardin [1] for soils was nothing else but the linear structural friction model that was introduced by Theodorsen and Garrick [2] when studying flutter. This model was later given the label *constant hysteretic model* by Bishop [3].

The constant hysteretic model is a pathological model because it is non-causal [4–7]. This means that the model responds prior to the application of an impulsive excitation. In fact, under an induced step strain there is as much response before the input as there is afterwards [6]. Accordingly, since the constant hysteretic model is physically unrealizable it cannot be expressed with a real-valued constitutive law in the time domain and traditionally it has been presented in the frequency domain in terms of its dynamic modulus

$$G(\omega) = G_1 + \mathrm{i}G_2 \operatorname{sgn}\left(\frac{\omega}{\varepsilon}\right) = G_1 \left[1 + \mathrm{i}\eta \operatorname{sgn}\left(\frac{\omega}{\varepsilon}\right)\right] \tag{1}$$

where G_1 is the frequency-independent storage modulus, $G_2 \operatorname{sgn}(\omega/\varepsilon)$ is the loss modulus, ω is the frequency variable; and ε is an arbitrary positive real number with units in rad/sec that is present to make the argument of the signum function dimensionless. The presence of the constant ε is imperative, since in this study the signum function is treated as a generalized function that is operated with the associated calculus [8]. On the right-hand side of (1), $\eta = G_2/G_1$, is the loss factor of the viscoelastic model given by Equation (1) and is also known as the hysteretic damping coefficient of the constant hysteretic element.

The appeal of frequency-independent dissipation generated by the constant hysteretic model motivated a number of researchers to adopt constant hysteretic dissipation in time-domain vibration analysis. Both real- and complex-valued formulations were considered [3, 9–11], all being limited to a single harmonic steady-state excitation. More recently, Bishop and Price [12] introduced the band-limited hysteretic dashpot and suggested that it might satisfy the causality requirement. However, Crandall [13] demonstrated that the band-limited hysteretic dashpot failed to satisfy causality.

The study reported in this paper was motivated by the challenge to address the issue of time-domain finite element analysis of soil structures without adopting the ad hoc approach of the Rayleigh damping approximation. The study elucidates the mathematical complexities associated with the concurrent requirements of frequency-independent dissipation and causality; and shows that in order to achieve physically realizable behaviour the requirement of a frequency-independent dissipation at the zero-frequency limit has to be abandoned.

TIME-DOMAIN VISCOELASTIC ANALYSIS

Commercially available computer software such as the program ABAQUS [14] allows for time-domain viscoelastic analysis provided that the constitutive law of the material is available in the time-domain under the integral representation

$$\tau(t) = \int_{-\infty}^{t} G_{\mathrm{R}}(t - \zeta)\dot{\gamma}(\zeta)\,\mathrm{d}\zeta \tag{2}$$

where $\tau(t)$ is the stress at the present time t, $\dot{\gamma}(\zeta)$ is the time history of the strain-rate and $G_R(t)$ is the relaxation modulus of the material that is defined as the resulting stress at the present time t due to a unit step strain at time ζ ($\zeta \leqslant t$).

Since the 'constant hysteretic model' initially proposed by Hardin [1] and subsequently used by Seed and Idriss [15], Veletsos and Verbic [16], Wolf [17] among others in non-causal, it does not posses a physically realizable relaxation modulus; and therefore a time-domain viscoelastic analysis using Equation (2) is not possible. Because of the need to analyse the transient response of soil structures, several popular ad hoc schemes have been proposed within the last 30 years to conduct time-domain finite element analysis of soil structures [18]. The most commonly utilized approach is to construct a consistent damping matrix, $[C]$, of the entire soil structure using the concept of Rayleigh damping where the damping matrix, $[C]$, is a linear combination of the mass matrix, $[M]$, and the stiffness matrix, $[K]$, of the entire structure

$$[C] = \alpha[M] + \beta[K] \tag{3}$$

in which α and β are frequency-independent coefficients. With this ad hoc approach the elements of the damping matrix $[C]$ can be constructed by using the information on the modal damping of the soil structure at two distinct modes. Assuming that $\{\phi_j\}$ is the jth natural vibration mode of the soil structure and that ω_j and ξ_j is the associated modal frequency and modal damping ratio, Equation (3) gives

$$\{\phi_j\}^{\mathrm{T}}[C]\{\phi_j\} = \alpha M_j + \beta\omega_j^2 M_j = 2\xi_j\omega_j M_j \tag{4}$$

in which $M_j = \{\phi_j\}^{\mathrm{T}}[M]\{\phi_j\}$. Equation (4) yields

$$\xi_j = \frac{1}{2}\left(\frac{\alpha}{\omega_j} + \beta\omega_j\right) \tag{5}$$

Parameters α and β are obtained by evaluating Equation (5) at two distinct modes; and the damping matrix, $[C]$, of the entire soil structure is constructed using Equation (3).

For a shear beam that consists of soil, and its dynamic shear modulus is approximated with the constant hysteretic model given by Equation (1), the modal damping ratios, ξ_j, assume the same value at all modes

$$\xi_j = \frac{\eta}{2} \quad \text{for all } j \tag{6}$$

It is important to emphasize that the modal damping ratio, ξ_j, appearing on the left-hand side of Equations (5) and (6) is a quantity that characterizes the entire soil structure; whereas, the hysteretic damping coefficient, $\eta = G_2/G_1$, appearing on the right-hand side of Equation (6) characterizes the dissipation of soil material at a point. It is partly because of the simple relation given by Equation (6) that the modal damping ratio and the hysteretic damping coefficient are often confused in the literature without distinguishing between the modal damping ratios of an entire structure, ξ_j, and the loss factor η, of a viscoelastic material.

The Rayleigh damping approach is a compromise that has been adopted because of the lack of a time-domain representation of the constant hysteretic model given by Equation (1). It can satisfactorily represent the damping level of soil structures at selected modes; however, it has been criticized that the high-frequency modes are artificially overdamped. For instance, Woodward and Griffiths [19] discuss the limitations of the Rayleigh damping approximation in computing the dynamic response of earth dams.

In this paper the problem of expressing the hysteretic behaviour of soil material within the context of linear viscoelasticity is addressed. Two causal hysteretic models, which are shown to be related, are examined and their performance in approximating the dynamic behaviour of soil is investigated. The first model is the causal hysteretic model which is a natural extension of the non-causal constant hysteretic model given by Equation (1). It is constructed by applying the Hilbert transform to the frequency-independent imaginary part [20]. The resulting relaxation modulus of the causal hysteretic model is zero at negative time, however is singular at the static limit (large time). This non-physical behaviour dictates that the only solution to obtain a physically realizable hysteretic model is to abandon the requirement of frequency-independent dissipation at the zero-frequency limit. A causal model that satisfies this requirement is the Biot model which was proposed more than 40 years ago [21]. Both causal models presented herein contain a free variable ε that emerges from the mathematical structure of hysteretic dissipation.

CAUSAL HYSTERETIC MODELS

The causal hysteretic model

The non-causal response of the constant hysteretic model was indicated as early as 1963 by Crandall [5]; however it was only until recently that the non-causality flaw of this model was rigorously addressed by Makris [20], who resolved this problem by investigating what was missing from the constant hysteretic model that makes it non-causal. He constructed the *causal hysteretic model* which has the same imaginary part as the *constant hysteretic model* but has the appropriate real part that makes the model causal. This requirement yields the following dynamic shear modulus [22]:

$$G(\omega) = G_1 + \frac{2}{\pi} G_2 \ln\left|\frac{\omega}{\varepsilon}\right| + \mathrm{i} G_2 \operatorname{sgn}\left(\frac{\omega}{\varepsilon}\right) \tag{7}$$

in which G_1, G_2, and ε are frequency-independent quantities while ω is the frequency variable. The causal hysteretic element given by Equation (7) was constructed by requiring that the real part (storage modulus), $G_1 + (2/\pi)G_2 \ln|\omega/\varepsilon|$, is the Hilbert transform of the imaginary part (loss modulus), $G_2 \operatorname{sgn}(\omega/\varepsilon)$. It is this very transformation that motivated the need to have a dimensionless argument, ω/ε, of the signum function. The dynamic modulus of the causal hysteretic element given by Equation (7) is nothing more than the familiar non-causal complex modulus given by Equation (1) [16, 23] enhanced with the term $(2/\pi)G_2 \ln|\omega/\varepsilon|$ in its real part in order to satisfy causality. Accordingly, the requirement for a frequency-independent loss modulus can be satisfied with a frequency-dependent storage modulus. The condition that the real and imaginary parts of a transfer function are Hilbert pairs ensures that the corresponding time-response functions of the model are zero at negative times. For instance, the relaxation modulus, $G_R(t)$, of the causal hysteretic model is [20]

$$G_R(t) = \left\{ \frac{G_1}{2} - \frac{G_2}{\pi}(\ln|\varepsilon t| + \gamma) \right\} [1 + \operatorname{sgn}(\varepsilon t)] \tag{8}$$

which is zero at negative times ($t < 0$), showing that the model given by Equation (7) is indeed causal. In Equation (8) $\gamma = 0.5772$ is the Euler constant. Defining the hysteretic damping coefficient,

$\eta = G_2/G_1$, Equation (8) reduces to

$$G_R(t) = G_1 \left[1 - \frac{2}{\pi}\eta(\ln|\varepsilon t| + \gamma)\right], \quad t > 0 \tag{9}$$
$$G_R(t) = 0, \quad t \leqslant 0$$

The arbitrary constant, ε, appearing in Eqs. (7)–(9) does not depend on the physics of the problem and can be set as small as desired so that the real part of Equation (7) matches a realistic storage modulus measured at some finite frequency.

The causal hysteretic element given by Equation (7) is physically realizable at finite frequencies; however, it is not defined at the static limit ($\omega = 0$). This negative singularity that the storage stiffness manifests at zero frequency is the outcome of the unrealistic requirement to have a frequency-independent loss modulus as frequency approaches zero (constant hysteretic damping). This unrealistic requirement assumes as infinite zero-shear-rate viscosity which is physically non realizable ($\mu = G_2/\omega$). Consequently, although the causal hysteretic element possesses a real-valued relaxation stiffness that is zero at negative times, its dynamic modulus is not defined at the static limit. This pathological behaviour is also reflected in the time domain since the relaxation modulus reaches negative values when εt is sufficiently large.

The foregoing discussion indicates that in order to construct a causal model that behaves properly at the static limit one has to abandon the requirement of a constant loss modulus in the vicinity of zero frequency. Such a nearly hysteretic model that satisfies causality was proposed by Biot more than 40 years ago; however, it did not receive the attention it deserves.

The Biot model

In a pioneering paper entitled 'Linear thermodynamics and the mechanics of solids', Biot [21], after first discussing fundamental concepts and properties in continuum mechanics, presented a hysteretic model that is the limiting case of a linear viscoelastic model consisting of a Hook element in parallel with an infinite number of Maxwell elements. This model is the continuous representation of the discrete Wiechert model [24]. Figure 1 shows a schematic analog of Biot's model that consists of a spring, G_1 in parallel with an infinite number of Maxwell elements with stiffnesses S_i and relaxation times λ_i. In a continuous representation the dynamic modulus of the model is Biot [21]:

$$G(\omega) = G_1 + \frac{2}{\pi}G_2 \ln\sqrt{1 + \left(\frac{\omega}{\varepsilon}\right)^2} + \mathrm{i}\frac{2}{\pi}G_2 \operatorname{atan}\left(\frac{\omega}{\varepsilon}\right) \tag{10}$$

in which G_1, G_2 and ε are frequency-independent constants and ω is the frequency variable. At the limiting case where $\varepsilon \ll \omega$, the function $\sqrt{1 + (\omega/\varepsilon)^2}$ tends to $|\omega/\varepsilon|$ and the function $\operatorname{atan}(\omega/\varepsilon)$ tends to $\pi/2$ showing that the causal hysteretic element given by Equation (7) is the high-frequency limit of Biot's model initially presented in 1958. This remarkable agreement between these two models that were constructed independently via different avenues demonstrates that there is continuous transition from linear viscoelasticity to purely hysteretic behaviour. It is interesting to note that the causal hysteretic model constructed by Makris [20], although pathological at the static limit, is the subtle mathematical link between the frequency-independent dissipation observed by Hardin [1] and the physically realizable hysteretic model proposed by Biot [21]. Figure 2 plots the real

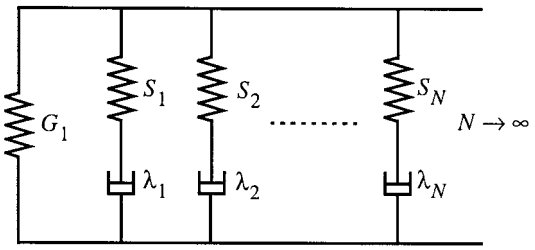

Figure 1. Schematic analog of Biot's linear hysteretic model.

and imaginary parts of the dynamic modulus of the three models given by Equations (1), (7) and (10) for $\eta = G_2/G_1 = 0.2$.

The time-domain behaviour of the Biot's model was investigated in depth by Caughey [4], who showed that its relaxation modulus is given by

$$G_R(t) = G_1\left[1 - \frac{2\eta}{\pi}E_i(-\varepsilon t)\right], \quad t > 0$$
$$G_R(t) = 0, \quad t \leqslant 0 \tag{11}$$

in which $\eta = G_2/G_1$ is again the hysteretic damping coefficient and $E_i(x)$ is the exponential integral [25]:

$$E_i(x) = \int_{\infty}^{-x} \frac{e^{-\xi}}{\xi}\, d\xi \tag{12}$$

The exponential integral kernel, $E_i(-\varepsilon t)$, appearing in Equation (11) is directly related to the kernel of the causal hysteretic element, $\ln|\varepsilon t| + \gamma$, appearing in Equation (9) via the identity

$$E_i(-\varepsilon t) = -E_1(\varepsilon t) = \ln|\varepsilon t| + \gamma + \sum_{n=1}^{\infty} \frac{(-1)^n(\varepsilon t)^n}{nn!} \tag{13}$$

Equation (13) shows that the kernels of the two models differ by the term $\sum_{n=1}^{\infty}(-1)^n(\varepsilon t)^2/nn!$, which vanishes when εt is sufficiently small ('recent past'). Figure 3 compares the relaxation modulus resulting from the Biot model (solid line) with the relaxation modulus of the causal hysteretic model given by Equation (8) dashed line. The constant hysteretic model is absent from Figure 3 since it does not possess a causal relaxation modulus.

In summary this section indicates that: (a) It is impossible to have a model with both frequency-independent loss modulus and frequency-independent storage modulus (constant hysteretic model is noncausal). (b) The causal hysteretic model has a frequency-independent loss modulus at the expense of a storage modulus which increases linearly with the logarithm of the frequency. This means that it has singularities at $\omega = 0$ and ∞. (c) In the Biot model both the loss modulus and the storage modulus vary with frequency. For low frequencies the storage modulus is essentially constant but the loss modulus varies linearly with frequency (Kelvin model). As the ratio ω/ε increases the Biot model exhibits a nearly frequency-independent dissipation at the expense of a

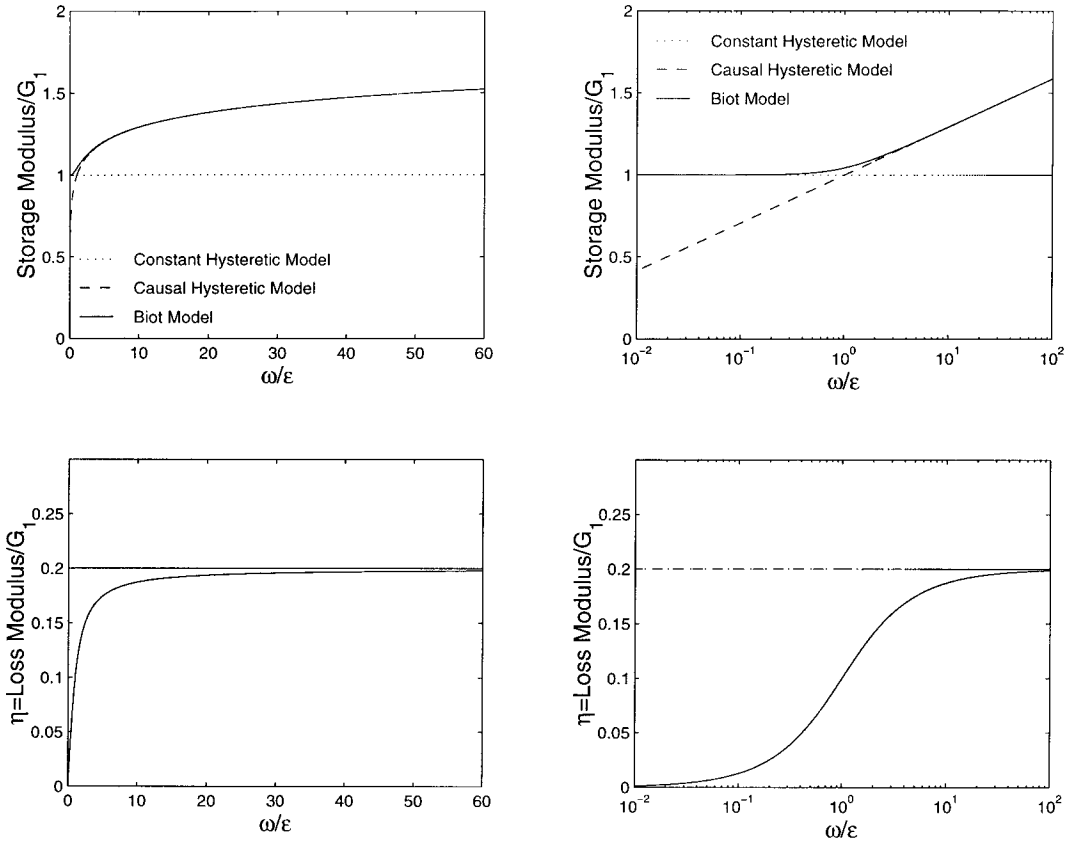

Figure 2. Real and imaginary parts of the dynamic stiffness of the Biot model (solid lines), the causal hysteretic model (dashed lines) and the constant hysteretic model (dotted lines). The three models are plotted in a linear frequency scale (left) and a logarithmic frequency scale (right).

storage modulus that increases linearly with the logarithm of the frequency. (d) At high frequencies (larger values of ω/ε) the Biot model approaches the causal hysteretic model.

Numerical implementation

The theoretical basis of numerical techniques which have been adopted to conduct time-domain viscoelastic analysis is that viscoelastic relaxation may be regarded as a superposition of elementary processes in which the stress relaxes exponentially with various relaxation times. Mathematically, such series are known as Prony or Dirichlet series [24]. For a solid-type Wiechert model (see Figure 1 with N being finite) the relaxation modulus is given by

$$G_{\mathrm{R}}(t) = G_1 + \sum_{j=1}^{N} S_j \, \mathrm{e}^{-t/\lambda_j} \tag{14}$$

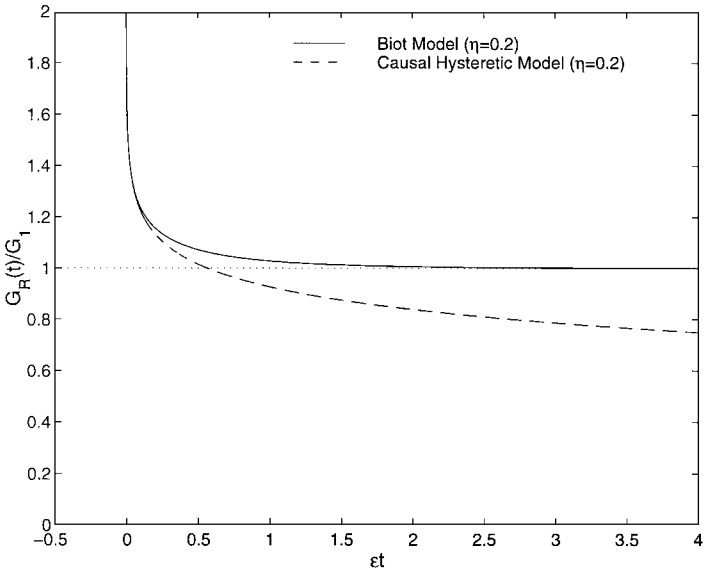

Figure 3. Relaxation stiffness of the Biot model (solid line) and of the constant hysteretic model (dashed line).

When Equation (14) contains sufficient terms it can approximate with fidelity any physically realizable relaxation process and commercially available computer software such as ABAQUS [14] provides entries for the spring stiffnesses, S_i, and the relaxation times λ_i in order to conduct time-domain finite element viscoelastic analysis. The set of model parameters S_i and λ_i is not unique and depends on the tolerance of the non-linear regression analysis that is used for parameter estimation. Denoting the normalized spring constants by $g_i = S_i/G_1$, the relaxation modulus given by Equation (14) takes the form

$$G_{\mathrm{R}}(t) = G_1 \left[1 + \sum_{j=1}^{N} g_j \exp\left(-\frac{\varepsilon t}{\varepsilon \lambda_j} \right) \right] \tag{15}$$

Since the Biot model is the continuous representation of the Prony series given by Equation (15), Equation (15) converges mathematically to Equation (11) as N increases [4]. For a given value of N the parameter g_i and $\varepsilon\lambda_i$ can be evaluated through a non-linear regression analysis and their resulting values are real and positive.

In the case of the causal hysteretic model Equation (15) is able to satisfactorily approximate the behaviour of Equation (9) when εt is sufficiently small. When εt assumes large values the relaxation modulus given by Equation (9) decreases monotonically below the static limit, G_1, and eventually become negative. This non physical behaviour cannot be captured with Equation (15) (Wiechert model) unless its parameters are allowed to assume negative values. Consequently, although the causal hysteretic element possesses a time-domain representation it cannot be replaced

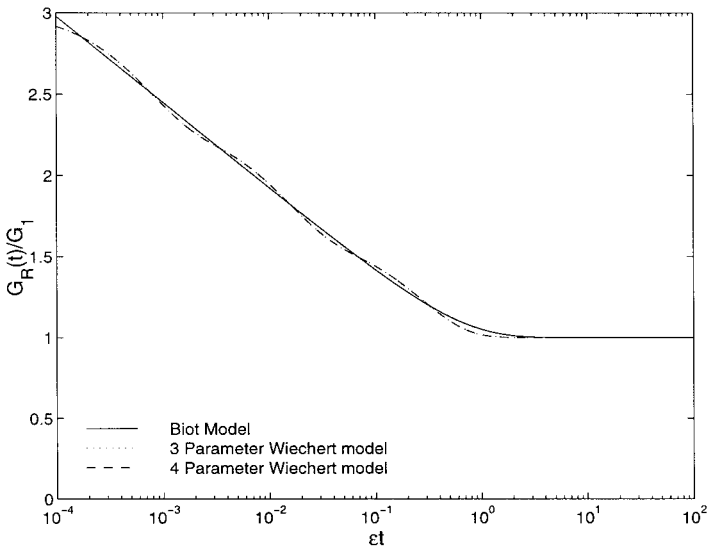

j	····· N=3		– – – – N=4	
	g_j	$\varepsilon\lambda_j$	g_j	$\varepsilon\lambda_j$
1	0.6282	0.2782	0.6301	0.2748
2	0.6975	0.0141	0.0024	0.0866
3	0.6979	0.0007	0.6873	0.0142
4			0.6955	0.0007

Figure 4. Approximations with Prony series of the relaxation stiffness of the Biot model ($\eta = 0.36$).

with a Prony series with parameters that assume physically admissible values. Figure 4 compares the results of Equation (15) when it approximates the relaxation modulus of the Biot model given by Equation (11) with $\eta = 0.36$. This value of damping constant is the appropriate damping level in the finite element analysis of a soil embankment that is presented later in the paper. The dotted line is obtained with $N = 3$; whereas the dashed line is obtained with $N = 4$. The parameters g_i and $\varepsilon\lambda_i$ used in each case are also shown in Figure 4. The performance of these parameters in approximating the dynamic modulus of the Biot model is shown in Figure 5.

Selection of parameter ε

In the previous section it was shown that the two causal hysteretic models have a frequency-dependent storage modulus and behave the same when ω/ε is large. The storage modulus of the Biot model is properly defined at the static limit; whereas, the causal hysteretic element given by Equation (7) results to a negative storage modulus when ω/ε is sufficiently small or to a negative

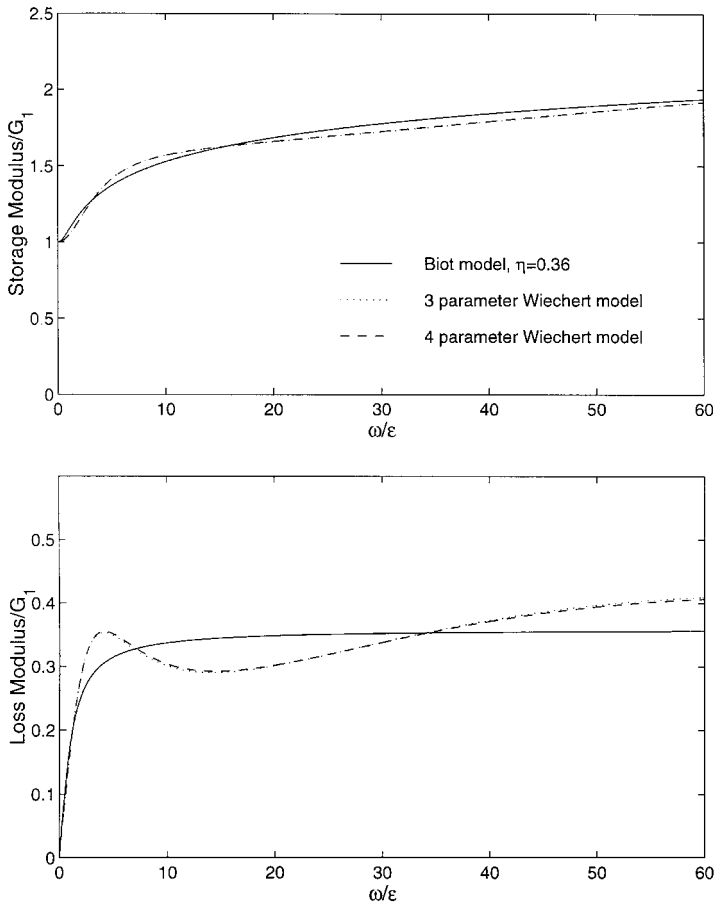

Figure 5. Comparison of the approximate dynamic stiffness that results from the Prony series with the dynamic stiffness of the Biot model ($\eta = 0.36$).

relaxation modulus when εt is sufficiently large. Herein we set as a condition that for the causal hysteretic model: (a) the resulting storage stiffness should be equal to the static shear modulus of the soil, G_s, at the smallest frequency involved in the analysis; and (b) the resulting relaxation modulus should assume the value of the static shear modulus, G_s, at a time that is as remote as the duration of the excitation, T_{ex}. The smallest frequency involved within the context of discrete Fourier transform analysis is, $\Delta\omega = 2\pi/T_{max}$, where T_{max} is the duration of the excitation augmented by the addition of a sufficient band of zeros at the end. The band of zeros has to be sufficiently long such that the response of the structure at the end of each cycle of a periodic extension of the excitation, T_{max}, is negligible. The longer the natural period of the structure or the smaller its damping, the longer will be the time needed for the free vibrational response to subside, and hence the longer the band of additional zeros.

From Equation (7) condition (a) gives

$$G_1\left(1+\frac{2}{\pi}\eta\,\ln\frac{\Delta\omega}{\varepsilon}\right)=G_s \tag{16}$$

By setting $G_s=G_1$, Equation (16) yields

$$\varepsilon=\Delta\omega=\frac{2\pi}{T_{max}} \tag{17}$$

From Equation (9), condition (b) gives

$$G_R(T_{ex})=G_1\left[1-\frac{2}{\pi}\eta(\ln|\varepsilon T_{ex}|+\gamma)\right]=G_s \tag{18}$$

which yields that

$$\varepsilon=\frac{1}{T_{ex}}\,e^{-\gamma} \tag{19}$$

The coexistence of conditions (a) and (b) gives that

$$T_{max}=2\pi e^{\gamma}T_{ex}\approx 11.19T_{ex} \tag{20}$$

This interesting relation implies that in order for the relaxation modulus of the constant hysteretic model to assume the static value, G_s, as recently as T_{ex} ago, the duration of the extended period, T_{max} has to be at least $2\pi e^{\gamma}\approx 11.19$ times the duration of the excitation T_{ex}. Parametric studies on the accuracy of the discrete Fourier transform method in predicting the response of structures subjected to pulse excitations indicated that in some cases the extended period T_{max} might have to be as long as the value given by Equation (20) [16]. Table I shows the minimum and maximum values that the storage and loss modulus of the three models under consideration assume over the entire frequency range of interest when $\varepsilon=\Delta\omega$. Clearly, the two causal models result to a stiffer representation at higher frequencies.

In the Biot model parameter ε can assume any positive value. Assuming that a transient excitation has a low dominant frequency, ω_d, Figure 2 (right) indicates that if $\varepsilon=\omega_d/10$, the loss modulus has assumed more than 90 per cent of its frequency-independent value, while the storage modulus is approximately 1.3 times its static limit. A larger value of ε (say, $\varepsilon=\omega_d$) keeps the storage modulus closer to its static limit, however the damping associated with the dominant frequency component of the excitation is half the frequency-independent value. In this case the model exhibits hysteretic damping only under the high-frequency content of the excitation.

PREDICTIONS OF HYSTERETIC MODELS

Herein the performance of the two hysteretic models introduced in the previous section is compared by investigating the response of an infinite long soil structure that can be approximated as a shear beam or a two-dimensional plane strain structure.

Assuming a horizontal base excitation, $\ddot{u}_g(t)$, and purely elastic behaviour, dynamic equilibrium of a slice of the shear beam with height, H, gives

$$\rho_s\frac{\partial^2}{\partial t^2}[u(z,t)+u_g(t)]=G_s\frac{\partial^2}{\partial z^2}u(z,t) \tag{21}$$

Table I. Normalized values of the real and imaginary parts of the three hysteretic models studied in this paper. In the two causal models $\varepsilon = \Delta\omega$.

	$G_1(\omega)/G_s$			$G_2(\omega)/G_s$		
	Constant hysteretic model	Causal hysteretic model	Biot model	Constant hysteretic model	Causal hysteretic model	Biot model
ω	1	$1+\frac{2}{\pi}\eta \ln\left\|\frac{\omega}{\varepsilon}\right\|$	$1+\frac{2}{\pi}\eta \ln\sqrt{1+\left(\frac{\omega}{\varepsilon}\right)^2}$	$\eta \operatorname{sgn}\left(\frac{\omega}{\varepsilon}\right)$	$\eta \operatorname{sgn}\left(\frac{\omega}{\varepsilon}\right)$	$\frac{2}{\pi}\eta \operatorname{atan}\left(\frac{\omega}{\varepsilon}\right)$
$\Delta\omega = \varepsilon$	1.0000	1.0000	1.0221	0.1000	0.1000	0.0500
$\frac{N}{2}\Delta\omega = 256\Delta\omega$	1.0000	1.3530	1.3530	0.1000	0.1000	0.0998
$\frac{N}{2}\Delta\omega = 512\Delta\omega$	1.0000	1.3971	1.3971	0.1000	0.1000	0.0999
$\frac{N}{2}\Delta\omega = 1024\Delta\omega$	1.0000	1.4413	1.4413	0.1000	0.1000	0.0999

where ρ_s and G_s are the density and elastic shear modulus of the soil material. The Fourier transform of (21) gives

$$\frac{G_s}{\rho_s}\frac{\partial^2}{\partial z^2}u(z,\omega)+\omega^2 u(z,\omega)=-\omega^2 u_g(\omega) \tag{22}$$

Application of the boundary conditions — that at the base the relative displacement, $u(0,\omega)=0$; and that at the crest the shear strain, $(\partial/\partial z)u(H,\omega)=0$, Equation (22) gives

$$u(z,\omega)=u_g(\omega)\left[\cos(kz)+\frac{\sin(kH)}{\cos(kH)}\sin(kz)-1\right] \tag{23}$$

where $k=\omega/V_s$ is the wave number and $V_s=\sqrt{G_s/\rho_s}$ is the shear wave velocity.

Under free vibrations ($u_g(\omega)=0$) the solution of Equation (22) gives the free vibration characteristics:

$$\omega_n=\frac{(2n-1)\pi}{2}\frac{V_s}{H} \tag{24}$$

$$\phi_n(z)=\cos\left(\frac{(2n-1)\pi}{2}\frac{z}{H}\right) \tag{25}$$

where ω_n are the natural frequencies and ϕ_n are mode shapes. Accordingly, the first natural period of the shear beam is $T_1=2\pi/\omega_1=4H/V_s$.

The frequency-domain response of a structure that consists of a viscoelastic material is given from the same equation that one derives by assuming a purely elastic material after replacing the

real shear modulus G_s with the constant shear modulus, $G_1(\omega)+iG_2(\omega)$. This is justified with the correspondence principle [26]. In the general case the presence of a complex shear wave velocity, V_s, results to complex natural frequencies, ω_n and complex mode shapes ϕ_n. In this study, the response of the shear beam is computed using the complex shear modulus for the soil given by Equations (1), (7) and (10).

The response of the shear beam subjected to a simple forward-and-back motion is investigated. A forward-and-back pulse can be expressed mathematically with a type-B pulse given Makris [22]

$$\ddot{u}_g^B(t) = \omega_p v_p \cos(\omega_p t), \quad 0 \leqslant t \leqslant T_p \tag{26}$$

$$\dot{u}_g^B(t) = v_p \sin(\omega_p t), \quad 0 \leqslant t \leqslant T_p \tag{27}$$

$$u_g^B(t) = \frac{v_p}{\omega_p} - \frac{v_p}{\omega_p}\cos(\omega_p t), \quad 0 \leqslant t \leqslant T_p \tag{28}$$

where v_p is the amplitude of the velocity pulse and $T_p = 2\pi/\omega_p$ is the duration of the pulse. Figure 6 (left) shows the acceleration, velocity and displacement histories of the fault-normal motion recorded at the El Centro Station Array #5 during the 15 October 1979 Imperial Valley earthquake. This motion resulted into a nearly forward-and-back pulse with a 3.2 sec duration. Figure 6 (right) plots the acceleration, velocity and displacement histories constructed with type-B pulse given by Equations (26)–(28) in which the values of $v_p = 0.7$ m/sec and $T_p = 3.2$ sec have been used. Figure 6 indicates that although the simple trigonometric pulse given by Equations (26)–(28) can capture many of the kinematic characteristics of some recorded near-source ground motions, it cannot capture the high-frequency fluctuations which are present in the acceleration history of the recorded motion.

Response analysis with the shear beam approximation

First response time histories with the shear beam approximation are computed by applying the inverse Fourier transform to the displacement transfer function given by (23)

$$u(z,t) = \frac{1}{2\pi}\int_{-\infty}^{\infty} u(z,\omega)e^{i\omega t}\,d\omega \tag{29}$$

Similarly the velocity, $\dot{u}(z,t)$ and acceleration histories $\ddot{u}(z,t)$ of the shear beam are computed by inverting in the time-domain the corresponding velocity and acceleration transfer functions. The forward Fourier transforms of the ground excitation and the backward Fourier transform of the response are computed with the FFT and IFFT routines available in MATLAB [27]. The excellent performance of the routine is shown in Figure 7 (top and centre) where the numerically computed Fourier transform of $u_g(t)$ given by Equation (28) is compared with the closed-form expression

$$u_g^B(\omega) = \int_{-\infty}^{\infty} u_g^B(t)e^{-i\omega t}\,dt = \frac{v_p}{\omega_p}\frac{i}{\omega}(e^{-2i\pi(\omega/\omega_p)} - 1)\left(\frac{1}{1-(\omega/\omega_p)^2}\right) \tag{30}$$

Figure 7 (bottom) plots the Fourier amplitude spectrum of type-B pulse and indicates that the low dominant frequency, $\omega_d = 2.2$ rad/sec, is slightly larger than the pulse frequency, $\omega_p = 2\pi/T_p = 1.96$ rad/sec.

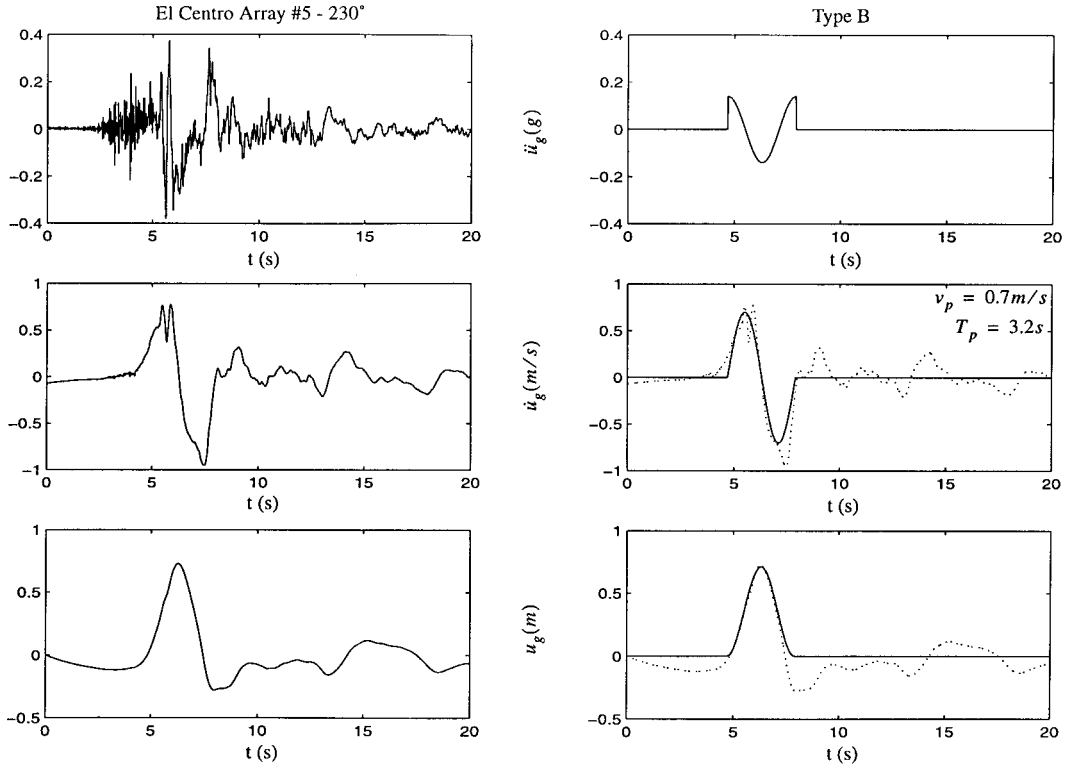

Figure 6. Fault normal components of the acceleration, velocity and displacement time histories recorded at the El Centro Array #5 station during the 15 October, 1979 Imperial Valley, California earthquake (left), and a cycloidal type-B pulse (right).

Within the context of equivalent linear analysis the non-linear behaviour of soil is expressed with strain-dependent modulus and strain-dependent damping coefficient curves. Figure 8 plots selected curves published in the literature based on the work of Seed and Idriss [15], Iwasaki *et al.* [28], Tatsuoka *et al.* [29], Vucetic and Dobry [30] among others. Note that in the bottom plot of Figure 8 the material damping of soil is presented in terms of $\eta = G_2/G_1$ and not in terms of ξ. Since the strain response is not known *a priori* iterations are required. Initially a strain level is projected, the associated shear modulus and damping coefficient are estimated and response time histories are computed. Seed and Idriss [15] suggested that 2/3 of the response strain should be used as the average strain to evaluate $G(\gamma)$ and $\eta(\gamma)$ for the next iteration. With a finite element analysis different values of soil parameters can be assigned at various locations according to the local strain [18]. With the frequency-domain formulation given by Equation (29) only a macroscopic value of an average strain $\hat{\gamma} = \hat{u}_c/H$ can be evaluated, where $\hat{u}_c$ is some representative crest displacement (say $\hat{u}_c = u_{c,\max}/2$) and H is the height of the shear beam. Figure 9 shows computed crest relative displacement, relative velocity and total acceleration histories of a

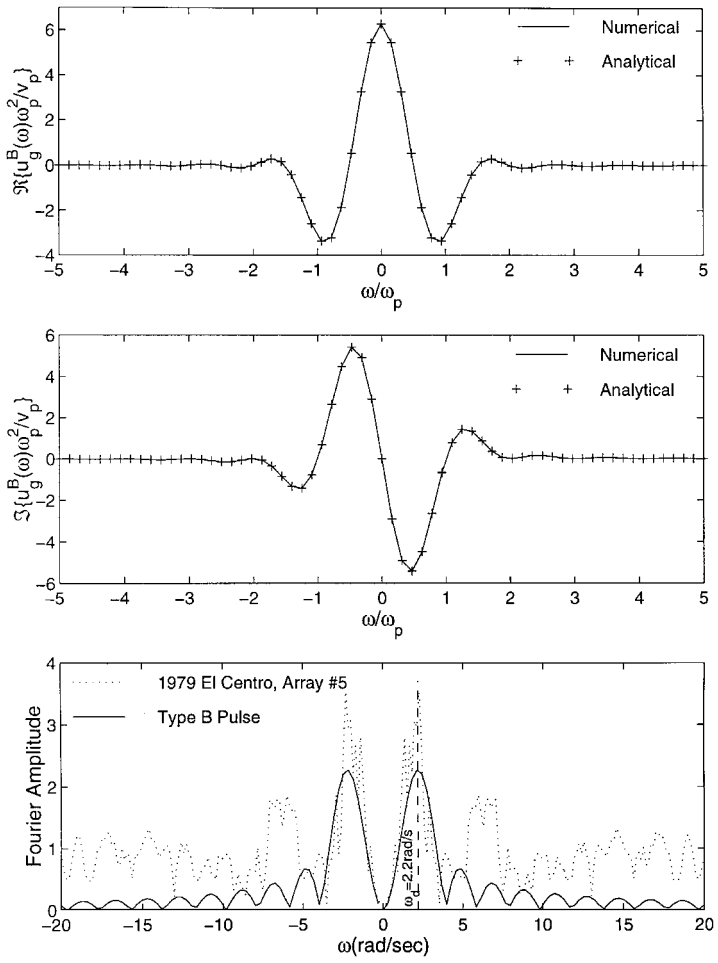

Figure 7. Real part (top), imaginary part (centre) and amplitude (bottom) of the Fourier transform of a type-B pulse. The Fourier amplitude of the El Centro 1979, Array #5 acceleration record is also shown with dotted line.

shear beam with height, $H = 10$ m and initial shear wave velocity $V_s = 150$ m/sec when subjected to type-B pulse motion shown on the right of Figure 6 ($T_p = 3.2$ sec, $v_p = 0.7$ m/sec). Assuming a soil density $\rho_s = 2$ Mg/m^3 the small-strain shear modulus $G_{max} = \rho_s V_s^2 = 45$ MPa. Following the Vucetic and Dobry [30] curve shown in Figure 8 which is for plasticity index, PI = 15, our analysis converged at an approximate strain 1.4×10^{-3} where $G/G_{max} = 0.35$ and $\eta = 0.26$. The response shown in Figure 9 was computed with the constant hysteretic model (left), the causal hysteretic model (centre) and the Biot model (right). The value of $\varepsilon = \Delta\omega = 0.1753$ rad/sec was computed with Equation (19) in which $T_{ex} = 3.2$ sec. The dotted line shown in Figure 9 is the

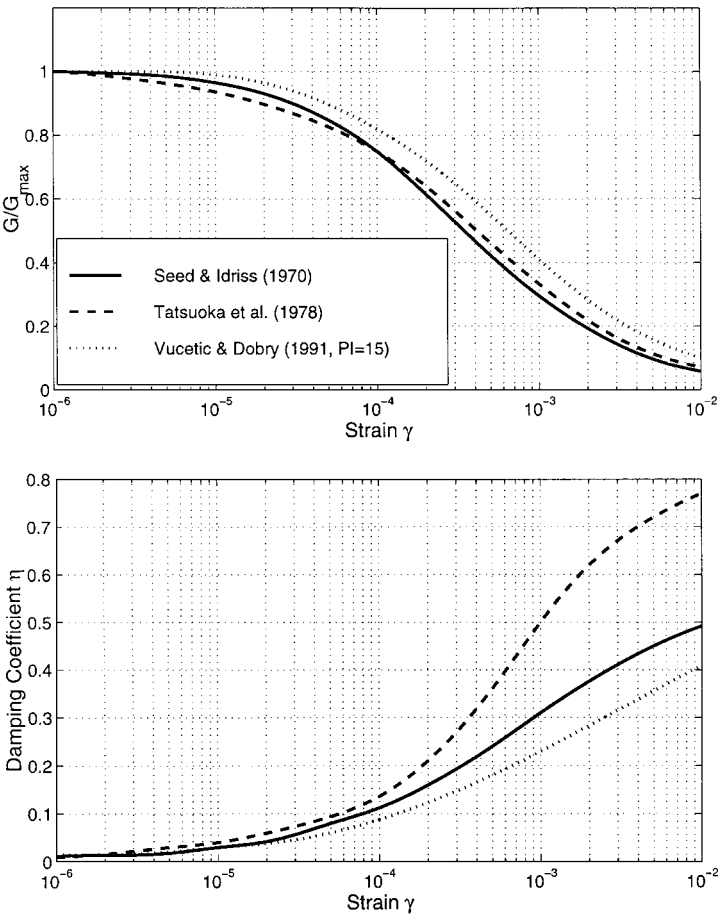

Figure 8. Normalized soil shear modulus and damping coefficient as a function of shear strain.

corresponding acceleration history at the base. The causal hysteretic model and the Biot model result in nearly identical responses which are at a slight higher frequency than the response obtained with the constant hysteretic model. This is because the storage moduli of the two causal models are increasing functions of frequency. In total the three models result in comparable responses. It is interesting to note that the velocity and displacement histories computed with the constant hysteretic model show an early rise before the initiation of the induced excitation, which is a manifestation of the non-causal nature of the model.

The frequency-domain computation of the shear-beam response allows for a direct comparison between the macroscopic predictions of the proposed hysteretic models and the traditional constant hysteretic model that has been used extensively to approximate soil behaviour. With this frequency-domain formulation all three hysteretic models discussed in this paper are applicable. However,

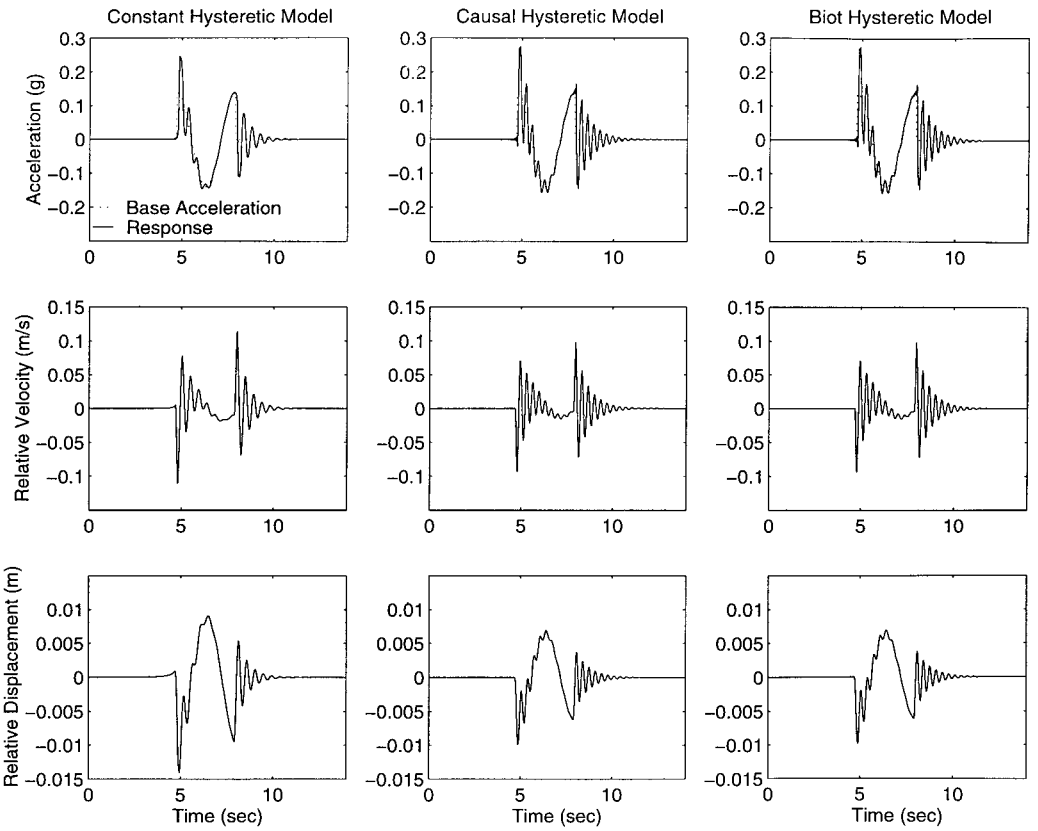

Figure 9. Crest total acceleration, relative velocity and relative displacement time histories computed with the shear beam approximation and the three hysteretic models ($\varepsilon = 0.1754\,\text{rad/sec}$) under a type-B pulse excitation. The response is computed with $G/G_{\max} = 0.35$ and $\eta = 0.26$.

the sophistication of this formulation is limited to the extent that a three-dimensional structure is approximated with a one-dimensional model.

Plane strain finite element analysis

When more detailed information on the response is needed, finite element analysis is conducted either following a modal superposition formulation or a direct time-integration formulation. In a modal superposition formulation the damping matrix of the structure $[C]$ is not needed; only the values of all the modal damping rations, ξ_j, need to be known at all vibration modes $\{\phi_j\}$ of interest. In a direct time integration formulation, the damping matrix, $[C]$ of the structure must be known in an explicit form and is usually constructed following the Rayleigh damping approximation outlined in the introduction of this paper. It is this kind of analysis that motivated the rigorous time-domain representation of the material damping of soil reported herein.

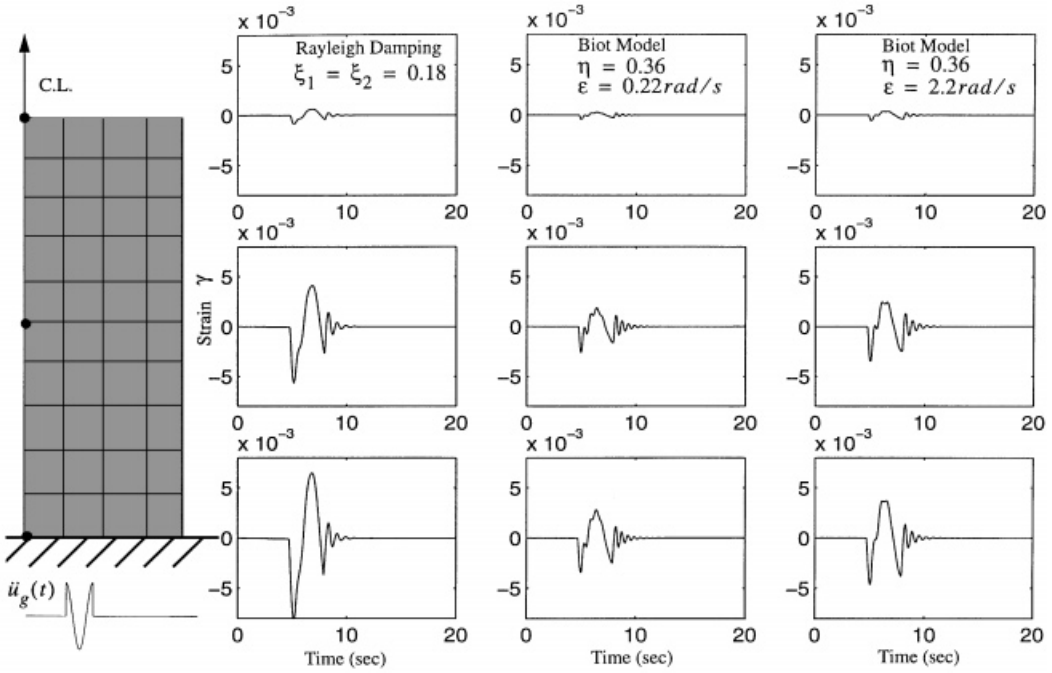

Figure 10. Strain time histories at the base, centre and near the top of a soil embankment computed with the Rayleigh damping approximation (left) and the Biot model (centre and right). Excitation: type-B pulse motion shown in Figure 6.

Figure 10 plots the time histories of the converged shear strains along the horizontal plane computed at the base, mid-height and crest of a rectangular soil embankment with $H = 10\,\text{m}$, $V_s = 150$ m/sec, and $\rho_s = 2$ Mg/m^3 subjected to type-B pulse shown on the right of Figure 6. During this first iteration the initial strain level was assumed 10^{-4} and according to the curves of Vucetic and Dobry [30] (PI = 15) the estimated values of shear modulus and damping coefficient are $G/G_{\max} = 0.82$, $\eta = 0.09$. At the last iteration $G/G_{\max} = 0.16$ and $\eta = 0.36$. The strain histories in the first column shown in Figure 11 are computed using the popular method that involves the Rayleigh damping approximation. The parameters α and β needed in Equation (3) are calibrated with Equation (5) by using that $\xi_1 = \xi_2 = \eta/2 = 0.18$, whereas the first and second modal frequencies were evaluated with the approximate Equation (24) to be $\omega_1 = 9.2$ rad/sec and $\omega_2 = 27.6$ rad/sec. For the last iterations the resulting values of $\alpha = 2.48$ sec^{-2} and $\beta = 9.80 \times 10^{-3}$ sec. The strain histories in the second and third column shown in Figure 10 are computed with a time-domain viscoelastic analysis using a four-term Prony series that approximates the relaxation modulus of the Biot model given by Equation (11). The parameters of the four-term Prony series used are shown in Figure 4. In computing the response shown in the centre column the value of $\varepsilon = 0.22$ rad/sec, that is equal to 1/10 times the dominant frequency of type-B pulse, $\omega_d = 2.2$ rad/sec. In computing the response shown in the right column of Figure 10 the value of $\varepsilon = \omega_d = 2.2$ rad/sec. With reference

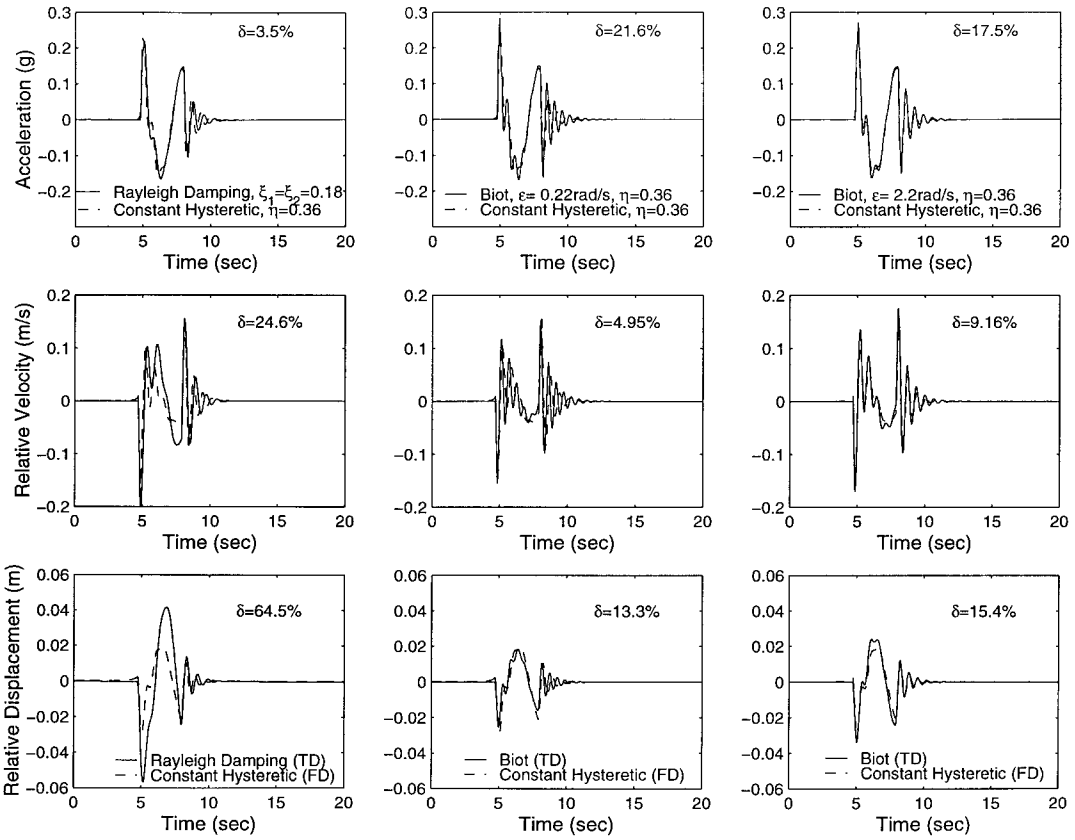

Figure 11. Crest total acceleration, relative velocity and relative displacement time histories computed with a two-dimensional finite element analysis using the Rayleigh damping approximation (left) and the Biot model (centre and right). The response computed with the constant hysteretic model via a frequency-domain analysis is also shown with a dashed line. Excitation: type-B pulse motion shown in Figure 6.

to Figure 2 the larger ε is, the closer the storage modulus is to the static value, G_1; and the smaller the loss factor is. This explains the slightly higher strain levels and the slower decay in the strain histories shown in the right column of Figure 10. The strain histories obtained with the Rayleigh damping approximation are more than 50 per cent larger than the strain histories obtained with the hysteretic model proposed by Biot.

Figure 11 plots the crest total acceleration (top) together with the crest relative velocity (centre) and the crest relative displacement (bottom) of the aforementioned soil embankment. The left column compares the results obtained from a two-dimensional time-domain analysis using the Rayleigh damping approximation ($\xi_1 = \xi_2 = 0.18$), with the results obtained from a one-dimensional (shear-beam) frequency-domain analysis using the constant hysteretic damping ($G/G_{\max} = 0.16$ and $\eta = 0.36$). The relative difference, δ, between the maximum values of a response quantity, say v,

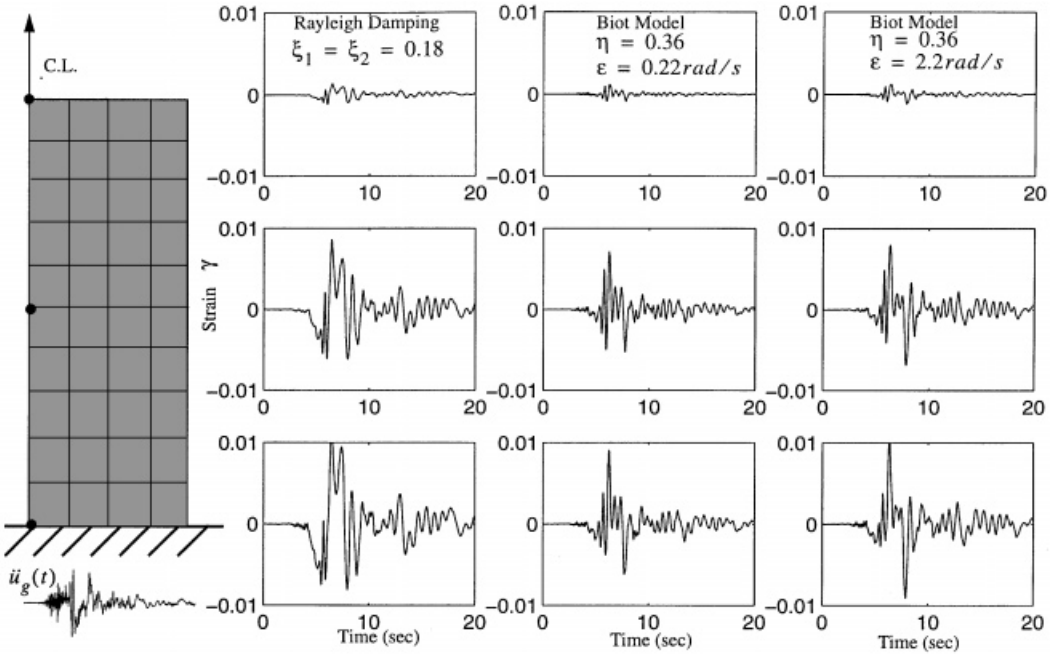

Figure 12. Strain time histories at the base, centre and near the top of a soil embankment computed with the Rayleigh damping approximation (left) and the Biot model (centre and right). Excitation: El Centro Array #5, 1979 Imperial Valley earthquake shown in Figure 6.

computed with the two idealizations is computed as

$$\delta = 2\frac{|v^{\mathrm{R}}|_{\max} - |v^{\mathrm{H}}|_{\max}}{|v^{\mathrm{R}}|_{\max} + |v^{\mathrm{H}}|_{\max}} \tag{31}$$

where $|v^{\mathrm{R}}|_{\max}$ and $|v^{\mathrm{H}}|_{\max}$ are the maximum response quantities computed with the Rayleigh damping and the constant hysteretic damping approximation, respectively. Figure 11 indicates that although in both models computed in the left column the percentage of damping is the same ($\xi_1 = \xi_2 = \eta/2 = 0.18$) and the peak accelerations differ only by 3.5 per cent, the difference in the computed relative displacement is more than 64 per cent. This large discrepancy in the computed displacements is mostly the result of the viscous nature that damping adopts with the Rayleigh damping approximation versus the hysteretic nature that is expressed with the constant hysteretic model. Under pulse-type motions it is known that the same percentages of viscous and rate-independent damping result in substantially different displacements of a single-degree-of-freedom structure [22, 31].

The centre column of Figure 11 compares the results obtained from a two-dimensional time-domain analysis using the Biot model ($\varepsilon = 0.22$ rad/sec) with the results obtained from a one-dimensional (shear beam) frequency-domain analysis using the constant hysteretic model ($G/G_{\max}$

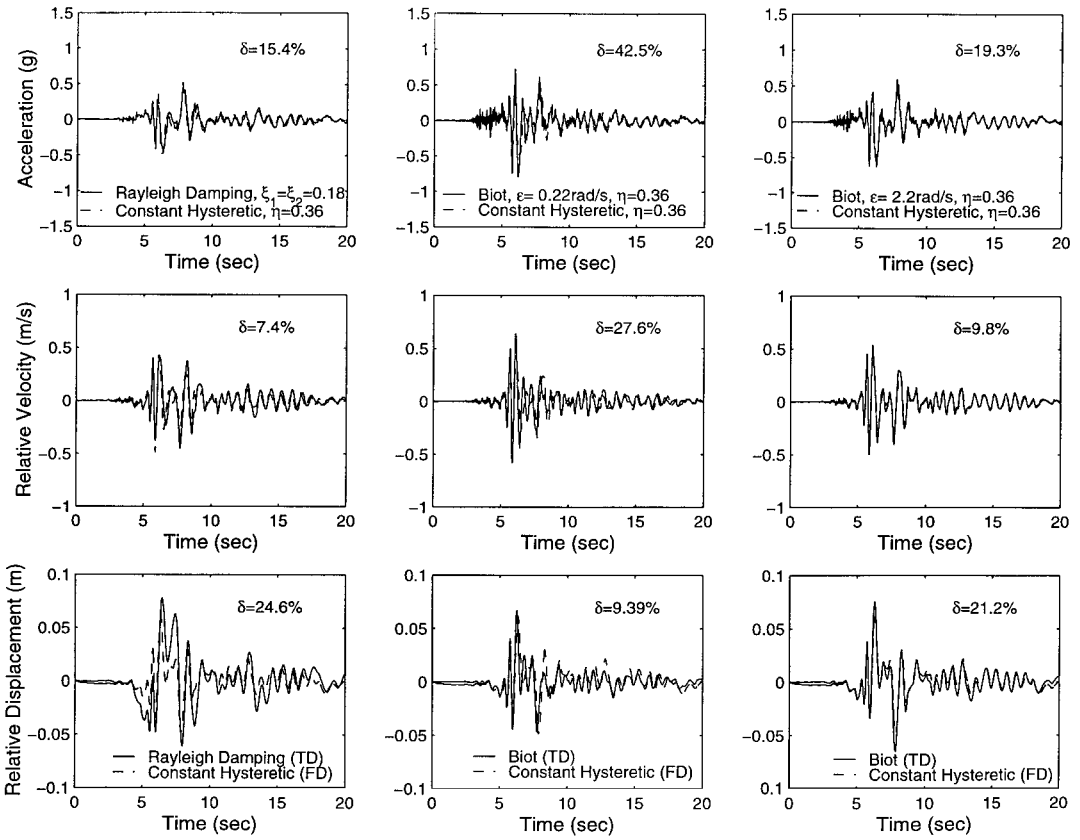

Figure 13. Crest total acceleration, relative velocity and relative displacement time histories computed with a two-dimensional finite element analysis using the Rayleigh damping approximation (left) and the Biot model (centre and right). The response computed with the constant hysteretic model via a frequency-domain analysis is also shown with a dashed line. Excitation: El Centro Array #5, 1979 Imperial Valley earthquake shown in Figure 6.

$= 0.16$ and $\eta = 0.36$). Now, although the relative difference, δ, between the maximum values of the crest accelerations predicted with the two hysteretic models is nearly 22 per cent, the relative difference, δ, between the maximum values of the crest displacements is less than 14 per cent. The computed response with $\varepsilon = \omega_d = 2.2$ rad/sec is shown on Figure 11 (right). In this case velocity and displacement maxima are slightly larger than those when $\varepsilon = \omega_d/10$, a result that is consistent with the strain histories shown in Figure 10.

In summary, this example shows that time-domain analysis of earth structures can be conducted rigorously within the context of linear viscoelasticity without adopting the Rayleigh damping approximations that imposes a non-appropriate viscous-type dissipation. The example shows that under pulse-type motions, the Rayleigh damping approximation overestimates displacements. This

can be avoided by conducting the time-domain finite element analysis with the Biot model and the proposed methodology.

Our study proceeds with the computation of the response of the same soil structure when subjected to earthquake excitation. Figure 12 plots the time histories of the converged strains at the base, mid-height and crest of the rectangular soil embankment with $H = 10$ m, $V_s = 150$ (m/sec) and $\rho_s = 2$ Mg/m^3 subjected to the Array #5 record of the 1979 Imperial Valley earthquake shown in Figure 6. At the last iteration the average strain converged at 5×10^{-3} resulting $G/G_{max} = 0.16$ and $\eta = 0.36$. The strain histories in the first column are computed with the Rayleigh damping approximation. The parameters α and β needed in Equation (3) are again calibrated with Equation (5). The strain histories in the second column shown in Figure 12 are computed with a time-domain viscoelastic analysis using the same four-term Prony series that was used earlier. The Fourier amplitude spectrum of the Array #5 record shown in Figure 7 indicates that the lowest frequency with a substantial concentration of energy is nearly the same to the dominant frequency of type-B pulse, $\omega_d = 2.2$ rad/sec. In computing the response shown in Figure 12 (centre) the value of the free parameter ε is taken equal to $\omega_d/10 = 0.22$ rad/sec. The response shown in the right column of Figure 12 is computed in the time domain using the Biot model with $\varepsilon = \omega_d = 2.2$ rad/sec.

Figure 13 shows that under earthquake excitation, the Rayleigh damping approximation yields results that are in closer agreement with the results obtained with hysteretic models. This is because under such excitation the embankment undergoes several cycles of shaking and the equivalent viscous damping approximation is more appropriate than when the excitation is a single pulse. Figure 13 also shows that the Biot model is capable to capture most of the details associated with hysteretic behaviour yet it allows for a time-domain finite element analysis. The presence of the free parameter, ε, allows for the computation of a family of solutions as ε assumes different positive values. The smaller ε is, the smaller is the excitation frequency at which the loss modulus assumes a nearly frequency-independent value; however, the stiffer the storage modulus becomes at higher excitation frequencies. Soil-strains associated with high-frequency motions are usually smaller; and the increased soil modulus predicted by Biot model is in agreement with the trends shown in Figure 8.

CONCLUSIONS

In this paper two causal viscoelastic models that evolved from the non-causal constant hysteretic model have been analysed in depth. The first model is the causal hysteretic model which has an imaginary part that is frequency independent the same way that is the imaginary part of the popular non-causal constant hysteretic model. The adoption of an imaginary part that is frequency independent even at the zero-frequency limit in conjunction with the requirement of causality resulted into a real part that is frequency dependent and singular at zero frequency. The causal hysteretic element, although not defined at the static limit, is the subtle mathematical link between the constant hysteretic model and the Biot model of viscoelasticity. In this study, after showing that the causal hysteretic element is merely the higher frequency limit of the Biot model we address the problem of conducting time-domain finite element analysis of earth structures without adopting the ad hoc Rayleigh damping approximation. It is shown that the Biot model is most suited for the numerical implementation of time-domain viscoelastic analysis since its discrete representation is a Prony series which can be directly implemented in commercially available computer software. The Biot model as well as the causal hysteretic model contains a free parameter ε that emerges from the

mathematical structures of frequency-independent dissipation. Theoretically, the free parameter ε in the Biot model can assume any positive value. Small values of ε result in a better approximation of an ideal hysteretic dissipation at the expense of an increase in the storage modulus. Larger values of ε result to a more rate-dependent dissipation with a storage modulus closer to its static limit. The paper shows that for pulse-type motions the Biot model yields more dependable results than the Rayleigh damping approximation which forces a viscous-type dissipation. In conclusion, the Biot model allows for a rigorous time-domain analysis within the context of linear viscoelasticity; yet it captures most of the hysteretic behaviour of earth structures and allows for the computation of their response when they assume any geometry.

ACKNOWLEDGEMENTS

This work is supported by the National Science Foundation Grant CMS-9696241 and the California Department of Transportation under Grant RTA-59A169. The valuable suggestions of the two anonymous reviewers are appreciated.

REFERENCES

1. Hardin BO. The nature of damping in sand. *Journal of Soil Mechanics & Foundation Engineering*, ASCE 1965; **91**:63–97.
2. Theodorsen T, Garrick IE. Mechanism of flutter, a theoretical and experimental investigation of the flutter problem. *NACA TR Rep. No. 685*, Natl. Advisory Com. for Aeronautics, Washington, D.C., 1940.
3. Bishop RED. The treatment of damping forces in vibration theory. *Journal of the Royal Aeronautical Society* 1955; **59**(539): 738–742.
4. Caughey TK. Vibration of dynamic systems with linear hysteretic damping (linear theory). *Proceedings of 4th U.S. National Congress Applied Mechanics*, ASME: New York, NY, 1962; 87–97.
5. Crandall SH. Dynamic response of systems with structural damping. In *Air, Space and Instruments, Draper Anniversary Volume*, Lees S (ed.). McGraw-Hill: New York, NY, 1963; 183–193.
6. Crandall SH. The role of damping in vibration theory. *Journal of Sound and Vibration* 1970; **11**(1):3–18.
7. Inaudi JA, Kelly JM. Linear hysteretic damping model and the Hilbert transform. *Journal of Engineering Mechanics*, ASCE 1995; **121**(5):626–632.
8. Lighthill MJ. *An Introduction to Fourier Analysis and Generalized Functions*. Cambridge University Press: Cambridge, U.K., 1989.
9. Myklestad NO. The concept of complex damping. *Journal of Applied Mechanics*, ASME 1952; **19**(3):284–286.
10. Reid TJ. Free vibration and hysteretic damping. *Journal of Royal Aeronautical Society* 1956; **60**:283.
11. Neumark S. Concept of complex stiffness applied to problems of oscillations with viscous and hysteretic damping. *Aero. Res. Council Rep. No. 3269*, 1957; 1–34.
12. Bishop RED, Price WG. A note on hysteretic damping of transient motions. In Random Vibration-Status and Recent Developments, Elishakoff I, Lyon RH (eds). Elsevier: Amsterdam, The Netherlands, 1986; 39–45.
13. Crandall SH. The hysteretic damping in vibration theory. *Proceedings of the Institution of Mechanical Engineers*, London, U.K. 1991; **205**:23–28.
14. ABAQUS. Hibbitt, Karlsson & Sorensen, Inc., 1997.
15. Seed HB, Idriss IM. Soil moduli and damping factors for dynamic response analysis. *Report No. EERC 70-10*, University of California, Berkeley, 1970.
16. Veletsos AS, Verbic B. Vibration of viscoelastic foundations. *Earthquake Engineering and Structural Dynamics* 1973; **2**:87–102.
17. Wolf JP. *Soil-Structure-Interaction in the Time Domain*. Prentice-Hall: Englewood Cliffs, NJ, 1988.
18. Idriss IM, Seed HB, Serff N. Seismic response by variable damping finite elements. *Journal of Geotechnical Engineering*, ASCE 1974; **100**(GT1):1–13.
19. Woodward PK, Griffiths DV. Influence of viscous damping in the dynamic analysis of an earth dam using simple constitutive models. *Computers and Geotechnics* 1996; **19**(3):245–263.
20. Makris N. Causal hysteretic element. *Journal of Engineering Mechanics*, ASCE 1997; **123**(11):1209–1214.
21. Biot MA. Linear thermodynamics and the mechanics of solids. *Proceedings of 3rd U.S. National Congress Applied Mechanics*, ASME: New York, NY 1958; 1–18.
22. Makris N. Rigidity-plasticity-viscosity: can electrorheological dampers protect base-isolated structures from near-source ground motions? *Earthquake Engineering and Structural Dynamics* 1997; **26**:571–591.

23. Kramer SL. *Geotechnical Earthquake Engineering*. Prentice-Hall: Upper Saddle River, New Jersey, 1996.
24. Tschoegl N. *The Phenomenological Theory of Linear Viscoelastic Behavior*. Springer: Berlin, 1989.
25. Abramowitz M, Stegun IA. *Handbook of Mathematical Functions*. Dover Publications, Inc: New York, NY, 1970.
26. Flugge W. *Viscoelasticity*. Springer: New York, 1975.
27. MATLAB. Math Works Inc., 1997.
28. Iwasaki T, Tatsuoka F, Takagi Y. Shear moduli of sands under cyclic torsional shear loading. *Soils and Foundations* 1978; **18**(1):39–56.
29. Tatsuoka F, Iwasaki T, Takagi Y. Hysteretic damping of sands under cyclic loading and its relation to shear modulus. *Soils and Foundations* 1978; **18**(2):25–40.
30. Vucetic M, Dobry R. Effect of soil plasticity on cyclic response. *Journal of Geotechnical Engineering*, ASCE 1991; **117**(1):89–107.
31. Makris N, Chang SP. Effect of damping mechanisms on the response of seismically isolated structures. *Report No. PEER-98/06*, Pacific Earthquake Engineering Research Center, November 1998.

